Platelet–Tumor Cell Hybrid Membrane-Camouflaged Nanoparticles for Enhancing Therapy Efficacy in Glioma

Lingling Wu
Zhejiang University School of Medicine Women's Hospital
Qin Li
Zhejiang Provincial People's Hospital
Junjie Deng
Wenzhou Institute of Biomaterials and Engineering: University of the Chinese Academy of Sciences Wenzhou Institute
Weide Xu
Wenzhou Institute of Biomaterials and Engineering: University of the Chinese Academy of Sciences Wenzhou Institute
Bingyu Chen
Zhejiang Provincial People's Hospital
Yaoqiang Du
Zhejiang Provincial People's Hospital
Wei Zhang
Zhejiang Provincial People's Hospital
Feihang Ge
Hangzhou Chinese Academy of Sciences-Hangzhou Medical College Advanced Medical Technology Institute
Siyun Lei
Zhejiang Provincial People's Hospital
Jinglan Shen
Zhejiang Provincial People's Hospital
Kaiqiang Li
Zhejiang Provincial People's Hospital
Zhen Wang (wangzhen@hmc.edu.cn)
Zhejiang Provincial People's Hospital https://orcid.org/0000-0002-8581-4649

Research Article

Keywords: glioma, hybrid membrane, biomimetic, β-mangostin, targeted delivery, anticancer

Posted Date: July 7th, 2021

DOI: https://doi.org/10.21203/rs.3.rs-664514/v1

Version of Record: A version of this preprint was published at International Journal of Nanomedicine on December 1st, 2021. See the published version at https://doi.org/10.2147/IJN.S333279.

Abstract

Cell membrane-camouflaged nanoparticles are drawing increasing attention because their surfaces retain the natural functionalities of the cell plasma membranes, making them a unique class of biomimetic materials combining natural and synthetic components. Modifying the cell membranes or combining the functions of different types of membranes enhances their functionality. Herein, we prepared platelet and tumor cell membrane camouflaged antitumor nanoparticles. The effects of β-mangostin-loaded nanoparticles on the target and its anticancer action in glioma were measured in vitro and in vivo. Multifunctional nanoparticles were manufactured with platelet–C6 hybrid biomimetic coating (PCM), lactic-co-glycolic acid (PLGA), and β-mangostin. PCM increased the proportion of active drug targeting in C6 and immune escape characteristics in THP-1 cells, thus enhancing the cytotoxicity of β-PCNPs. The β-PCNPs were comprehensively characterized to study the inherent properties of both source cells. Compared with bare β-NPs, β-PCNPs exhibited high tumor-targeting ability and induced apoptosis of C6 cells in vitro. Mice experiments with intravenous administration of the drug revealed that the β-PCNP platform enhanced the tumor targeting capability and exhibited excellent chemotherapy with high inhibition rate of glioma tumor growth in vivo. The mice in the β-PCNP group had a markedly prolonged circulation lifetime and exhibited better outcome than those in the β-NP group. These results provide a new strategy of utilizing PCNPs as carriers for drug delivery, which improves the targeting efficiency and therapeutic efficacy of chemotherapeutic agents for glioma therapy.

1. Introduction

Glioblastoma multiforme (GBM) is the most common and aggressive malignant tumor of the central nervous system, with extremely high mortality rate[1]. Despite surgical resection in conjunction with current adjuvant therapies, it remains highly lethal, and the median survival period for GBM patients is presently only 14.6 months, with a 5-year survival rate of approximately 5%[2]. To improve the chances of survival, chemotherapy is often administered to patients as adjuvant treatment[3]. During the course of chemotherapy, the blood–brain barrier (BBB) and blood–brain tu mor barrier (BBTB) constantly interact and affect the environment for the treatment of the tumors, which largely restricts efficient drug delivery to the glioma and reduces the therapeutic effects of glioma intervention[4]. Driven by these circumstances, the development of deliverable therapeutic agents that can cross physiological and pathological barriers is urgently needed for the treatment of the glioma.

Nanoparticle (NP)-based drug delivery systems have become a promising tool for improving the delivery and effectiveness of therapeutic drugs for tumors[5 6]. Poly (lactic-co-glycolic acid) (PLGA) is an excellent drug carrier owing to its biocompatibility, biodegradability, and toxicologically safe degradation products, and has been widely used in drug delivery[7]. Studies have extensively documented the functionalization of PLGA via various targeting ligands, such as peptides, antibodies, and nucleic acids[8]. Nonetheless, the poor passive targeting ability and relatively short circulation time of the nanocarriers limit their clinical

application [9]. However, nanomaterials are easily intercepted by macrophages, thereby triggering weak immunocompatibility[10].

Nature-inspired biomimetic nanocarriers are expected to improve the current drug delivery applications[11]. In recent years, natural cellular membranes, including red blood cell[12], white blood cell[13], platelet[14], macrophage[15], and cancer cell[16] membranes, have been used to create membrane materials. Cell membrane-based biomimetic nanomaterials, while retaining the bioengineering flexibility of the core, functionalize the NPs with various cellular membrane strategies that endow the nanomaterials with many desirable features[17]. In order to overcome the functional limitations of single-cell membranes to enhance the functionality of the nanomaterials, researchers have developed specialized platforms by camouflaging the NPs with hybrid membranes, formed by fusing membranes from different types of cells such as red blood cells and cancer cells [18], platelets and red blood cells[19], and cancer cells and macrophage membranes[20]. However, hybrid cell membrane formed by combining the platelet and glioma cell membrane materials have not been fabricated heretofore. In this study, we developed tumor-targeting NPs through suitable tactics to enhance the efficacy of cancer therapy. The NPs consist of platelet and tumor membranes and a drug, and demonstrate excellent targeting and immune escape capabilities.

Compared with traditional chemotherapeutics, natural fruit extract has the characteristics of less toxicity, high drug compliance, and favorable antitumor efficiency[21–23]. β-Mangostin, a xanthone originated from the pericarp of Garcinia mangostana Linn, has several bioactivities and pharmacological properties[24]. Previous reports have indicated that β-mangostin has anticancer activity against diverse cancer types including hepatocellular carcinoma [25], melanoma[26], and cervical cancer[27]. Our previous study found that the major component of the Garcinia mangostana L. extract, β-mangostin, has excellent anti-glioma effects, which could cause C6 oxidative damage-induced cell death in glioma cells through PI3K/AKT/mTOR pathway inhibition[28]. However, the aqueous solubility, tumor target selectivity, and BBB rate of β-mangostin does not meet clinical requirements.

Considering the above, we synthesized β-mangostin-loaded platelet–C6 cell hybrid biomimetic membrane camouflaged-PLGA NPs (β-PCNPs) for targeting cancer. In this work, we studied the effects of the biomimetic properties, namely the interface potential and biological activity, of β-PCNPs, through systematic evaluation both in vitro and in vivo in a xenograft mouse model and an orthotopic glioma model.

2. Materials And Methods

2.1 Materials

C6 cells, HT22 cells, human THP-1 cells (the Chinese Academy of Sciences Cell Bank); Garcinia mangostana L. (Thailand); poly (lactic-co-glycolic acid) (PLGA, Lactel Absorbable Polymers); platelet-rich

plasma (provided by volunteers), BALB/Nude mice (Shanghai SLAC Laboratory Animal Co., Ltd.); mannitol, sucrose, Tris/HCL, $MgCl_2$, KCL, DiD, DiO, DiI, phorbol myristate acetate (Sigma Aldrich); protease inhibitor cocktail (Bimake, Shanghai); phosphate buffered saline (PBS, Sigma Aldrich); BCA protein kit, CCK8 kit (Beyotime, China); paraformaldehyde (Sigma, USA); FBS, penicillin–streptomycin (Gibco, USA); DMEM, RPMI 1640 (Hyclone, Shanghai).

2.2 Preparation of β-Mangostin-Loaded NPs

Ten kilograms of fresh Garcinia mangostana L. were separated and chopped, and dried for a week. The peel was pressed into a powder, and β-mangostin (13.4 mg) was obtained by chromatography. β-NPs were prepared using the ultrasonic emulsification solvent evaporation method. PLGA (20 mg) dissolved in ethyl acetate (500 μL), and β-mangostin (2 mg) dissolved in 200 μL DMSO, were used as the organic phase. The mixture was poured into 2 ml 1.5% polyvinyl alcohol (PVA) for ultrasonic treatment on ice for 10 min to form colostrum. Then, 2 ml of 0.5% PVA was added to the mixture for ultrasonic treatment on ice for another 10 min to form a well-dispersed compound emulsion. The mixture was stirred for 5 h at room temperature (1000 rpm) until the organic solvent was completely volatilized. The collected NPs were centrifuged at 4°C and 18000 g for 15 min, and washed three times, and then the obtained yellow NPs were stored at − 80°C.

2.3 Extraction of Platelet Membrane and C6 Cell Membrane

Human platelet membranes were derived from platelet-rich plasma provided by volunteers. To obtain the purified platelet membrane, the obtained platelets was centrifuged at 4°C and 100 g for 15 min. The supernatant was centrifuged at 4 ℃ and 800 g for 20 min. Then, the lysis buffer (25 mM sucrose, 75 mM mannitol, 1 mM KCl, 10 mM Tris/HCl, 1 mM $MgCl_2$) and protease inhibitor (1000×) were added, followed by resting on ice for 15 min. The platelets were repeatedly frozen and thawed five times. After the last freeze–thaw cycle, the platelets were processed in an ultrasonic crusher for 5 s, and the process was repeated five times at intervals of 5 s. The platelets were then centrifuged at 21000 g for 10 min, re-suspended in PBS, and stored in a refrigerator at − 40°C.

The C6 cells were incubated and collected, and then cells at a density of 1×10^7 were suspended in 5 mL of lysis buffer containing 50 μL protease inhibitor cocktail. After being placed in an ice bath for 20 min, the C6 cells were repeatedly frozen and thawed five times. Later, the cell lysate was centrifuged at 2000 g for 15 min at 4°C, and the collected supernatant was further centrifuged at 21000 g for 30 min. Finally, the white precipitate containing the plasma membrane was stored at − 40°C for the subsequent experiments.

2.4 Preparation and Characterization of Hybrid Membrane Coated NPs

DiD (10 mg/mL) and DiO (10 mg/mL) were added to PLTM and C6M suspensions, respectively, and incubated for 1 h at room temperature on a shaking table. After centrifugation at 4°C and 21000 g for 10 min, the free dye was removed, and DiD-labeled PLTM and DiO-labeled C6M were obtained. Five hundred

microliters of each solution was mixed and pushed 11 times using the liposome extruder, and another 500 μL of each solution was mixed to obtain PLTM&C6M solution. Finally, the two solutions were placed on glass slides and imaged under a confocal laser scanning microscope (CLSM).

The composite cell membrane solution PLT-C6M obtained by the above method was mixed with the β-NPs and kept overnight. The liposome extruder was used to push the solution 11 times through polycarbonate membranes of 400 nm and 200 nm. Thus, membrane-coated NPs loaded with β-mangostin were obtained. The sizes and zeta potentials of the prepared membrane-coated NPs were characterized using a Zetasizer. For transmission electron microscopy (TEM), 10 μL of 0.2 mg/mL TEM sample was added onto the carbon-coated grid after being cleaned by plasma. Then the grid was rinsed with deionized water. 10 μL of 2% uranyl acetate solution in water was dropped on the grid for 2 min and removed via filter paper. The staining step was repeated three times prior to the sample imaging with TEM operating at 200 KV.

2.5 In Vitro Stability of NPs and Drug Release of β-PCNPs

To evaluate the stability of the NPs, the PCNPs were suspended in water, 1×PBS, and 10% fetal bovine serum at a final concentration of 1 mg/mL. One week after the set time point, the sample size was determined using the Zetasizer to test the aggregation. The prepared β-NPs and β-PCNPs were placed in a dialysis bag (MWCO = 12–14 kDa), and 30 ml of the solution (H_2O, PBS, and 10% FBS) containing 0.1% Tween 80 was added to a 50 ml centrifuge tube. The physiological environment in vivo was simulated on a shaker at 37°C and 200 rpm. After a predetermined time (0, 2, 4, 8, 24, 48, 72, 96, 120, 144, and 168 h), all the solutions were extracted and replaced with 30 ml of the same solution. The absorbance of the released β-mangostin was measured at 360 nm using a microplate reader.

2.6 Active Targeting and Immune Escape Characteristics of PCNPs

The cellular uptake of C6 cells and macrophages was quantitatively analyzed by laser scanning confocal microscopy (LSCM) and flow cytometry. C6 cells were seeded on a 6-well plate at a density of 5×10^5 cells per well and cultured for 12 h. THP-1 cells were maintained in RPMI 1640 medium supplemented with 10% FBS and 1% penicillin–streptomycin at 37% and 5% CO_2. The cells were differentiated into macrophage-like phenotype cells by culturing them with 100 ng/mL phorbol myristate acetate(PMA) for 48 h. Fluorescently labeled NPs were synthesized by incorporating 0.1 wt% DiD into the PLGA cores. The cell culture media were then replaced with fresh media containing NPS, PNPs, CNPs, and PCNPs. At 4 h after incubation, the cells were washed twice with PBS and fixed with pre-cooled 4% paraformaldehyde in PBS for 15 min, labeled with DAPI for 15 min, and then washed thrice with PBS. Finally, 10 μL of an anti-fluorescence quenching agent was added to the cell slide. Cellular fluorescence was observed using CLSM. After internalization, the adherent cells were further digested into a single cell suspension by trypsin digestion, suspended in 0.5 mL of PBS (0.01M, pH7.4), and analyzed by flow cytometry.

2.7 In Vitro Anti-tumor Performance

We evaluated the cytotoxicity of the nanoscale systems against C6 cells and mouse hippocampal neurons HT22 by using an in vitro CCK8 kit assay. First, we evaluated the toxicity of PCNPs on HT22 cells. Briefly, the HT22 cells were inoculated in 96 well plates at a density of 1.0×10^4 cells per well and cultured in a CO_2 incubator for 24 h. The old culture medium was discarded, and 100 μL of PCNPs of different concentrations (2, 4, 8, and 16 mg/ml) was added into the well plate and incubated for 24 h. The well without the sample was considered the control group, and the well without cell and sample was considered the blank group. Before the CCK8 experiment, the medium in each well was removed and washed three times with 1×PBS. CCK8 (10 μL) was added to each well, and the plates were incubated in an incubator for 1–4 h. The absorbance at 562 nm was measured using a microplate, and the cell survival was calculated. The CCK8 kit was also used to evaluate the cytotoxicity of β-mangostin-loaded NPs coated with different cell membranes on the C6 cells. The C6 cells were seeded in 96-well plates at a density of 1.0×10^4 cells per well and cultured for 24 h. Then, the NP solutions (NPs, PNPs, CNPs, PCNPs) loaded with different concentrations of β-mangostin (5, 10, 15, 20, and 25 μg/ml) was added to the corresponding pore plates and incubated for 24 h; the pores without samples were considered the control group, and the pores without cells and samples were considered the background group. Cell viability was evaluated as described above.

2.8 In vivo Anti-tumor Performance in Subcutaneous Glioma Model

All animals were raised in a specific pathogen free environment. This project was approved by the Medical Ethics Committee of Zhejiang Provincial People's Hospital. We acknowledge that the project was performed according to international, national, and institutional rules for animal experiments, clinical studies, and biodiversity rights. C6 cell suspension in good condition was collected and used to construct a subcutaneous tumor model in mice. The cell suspension was diluted to 5×10^6 cells/mL according to the volume ratio of the cell suspension : matrix gel = 2:1. Sixty 4-week male BALB/Nude mice (18–22 g) were randomly divided into six groups of 10 mice each. A C6 cell suspension (200 μL) was injected into the subcutaneous tissue of the right back of each nude mouse. When the tumor volume reached approximately 80–100 mm^3, the mice were treated with PBS, β-mangostin, β-NPs, β-PNPs, β-CNPs, and β-PCNPs every other day at the same dose (5 mg/kg, 200 μL). Totally, seven doses were administered. The weight and tumor growth of the nude mice were monitored every two days after the first injection. The tumor volume was measured using a Vernier caliper, and the volume was calculated according to the formula $V = (length \times width^2)/2$. On the 18th day, the mice were sacrificed for biochemical and pathological analyses and toxicological evaluation. The tumor was stripped, weighed, and photographed.

2.9 In Vivo Imaging of the Animals

We used the Xplore Optix MX animal optical molecular imaging system to image the healthy BALB/C nude mice to obtain the distribution of the NPs in vivo and their accumulation in the brain regions. The imaging system used 580 nm excitation and 692 nm emission wavelengths. To establish the C6 intracranial orthotopic glioblastoma mouse model, the mice were anesthetized using 3.5% chloral hydrate

(1.5 mL/100 g body weight). The head (the area to be inoculated) was cleaned with 70% ethanol and then opened with a sterilized scalpel. Five microliters of the C6 cell suspension (1×10^5 in 10% DMEM) was injected into the striatum at a depth of 3 mm from the dural surface. Twenty days after the orthotropic glioma model was established, the mice were randomly divided into four groups and each nude mouse was injected with 200 μL of DiD-labeled NPs, PNPs, CNPs, and PCNPs via the tail vein. At 24 h after injection, the mice were anesthetized with isoflurane and imaged from the back.

2.10 In Vivo Anti-tumor Performance in Orthotopic Glioma Model

All animal experiments were conducted in accordance with the guidelines approved by the Laboratory Animal Management and Ethics Committee of Zhejiang Provincial People's Hospital. An orthotropic glioma model was constructed according to the above method. Seven days after the model was established, the mice were randomly divided into six groups (PBS, β-mangostin, β-NPs, β-PNPs, β-CNPs, β-PCNPs) and administered the same dose and injection as the mice with the subcutaneous tumor. The overall survival was monitored in all groups. On the 20th day after modeling, one mouse was randomly selected from each group, and the brains and major organs were sampled for H&E staining. The remaining mice in each group were observed until their death.

2.11 Statistical Analysis

All statistical tests were analyzed by GraphPad Prism 8 software, and the comparison between the groups was performed by unpaired t-test; the results of more than three independent repeated experiments were expressed as mean ± SEM. $P < 0.05$ was the statistical difference between the groups, denoted by *; $P < 0.01$ was the statistically significant difference, denoted by **; $P < 0.001$ was the statistically significant difference, denoted by ***.

3. Results

3.1 PLT–C6 Hybrid Cell Membrane Characterization.

As shown in Fig. 1A, as the amount of C6 membrane increased in comparison with the PLT membrane, there was a recovery of fluorescence at 590 nm, whereas the fluorescence gradually decreased at 670 nm. This indicated the weakening of the FRET interaction in the hybrid PLT-C6 cell membrane due to the interspersing of the two membrane materials. Additionally, a PLT–C6 hybrid membrane was fabricated by using a 1:1 protein mass ratio of the PLT cell membrane labeled with DiD and C6 cell membrane labeled with DiI as a precursor. The PLT cell membranes labeled with DiD appeared red and the C6 glioma membranes incubated with DiI appeared green. It is clear that the data shown in Fig. 1B indicate a significant merging of the fluorescent signals derived from DiD and DiI. In vivid contrast, the mixture of the PLT membrane and C6 membrane constructed with the individual fluorescent dye-labeled membrane exhibited distinct red and green light spots. These results suggest the successful fusion of the natural PLT membrane and C6 cell membrane.

3.2 Preparation and Characterization of PCNPs.

PLTM, C6M, and PLTM-C6M were wrapped within the nanocarrier using the cell membrane extrusion method to obtain PNPs, CNPs, and PCNPs, respectively[29]. As shown in Fig. 1C, the TEM images of the PCNPs negatively stained with uranyl acetate showed hollow, spherical particles with a diameter of 130 nm, with a uniform approximately 10-nm-thick outer shell that was indicative of a hybrid membrane; the results were consistent with the size results in Fig. 1F. Furthermore, dynamic light scattering (DLS) showed that the PCNPs were larger than the bare core NPs (131.7 Â nm vs. 121.9 Â nm; Fig. 1D), and the surface zeta potential changed from − 43.9 mV to − 10.3 mV after the hybrid membrane coating (Fig. 1E), thereby confirming the presence of a charged outer membrane layer similar to that of the PLT–C6 hybrid cell membranes. As shown in Fig. 1G, the protein markers in the hybrid PLT–C6 membrane were inherited from the membranes of the platelets and C6 glioma cells, indicating successful extraction of the membranes. Thus, the PLT–C6 hybrid membrane was successfully prepared and coated onto the PLGA NPs.

3.3 Active Targeting and Immune Escape Characteristics of PCNPs

Imaging was done on confocal laser-scanning microscope (Fig. 2A). After incubation of the cells with DiD-PCNPs for 4 h, DiD was mainly localized in the cytoplasm of the C6 glioma cells and showed brighter red fluorescence than the NP-treated cells. C6 cell uptake was further investigated using flow cytometry (Fig. 2B-C). DiD fluorescence intensity in the C6 cells treated with DiD-PNPs and DiD-CNPs was approximately 1.9 times stronger than that of cells treated with bare DiD-NPs, whereas the C6 cells treated with DID-PCNPs were approximately 3.1 times stronger than those treated with bare DiD-NPs, indicating that platelet and C6 glioma cell membrane-coated NPs have good target recognition characteristics for tumor cells. In addition, to evaluate its antiphagocytic properties, the internalization of DiD-PCNPs by macrophages was tested by CLSM imaging. As shown in Fig. 2D, only a very low level of red fluorescence in the C6 treated with DiD-PCNPs, which appeared weaker fluorescence than the DiD-NP-treated group. Quantitative analysis by flow cytometry suggested that the fluorescence intensity in the DiD-NP group was 2.3-fold stronger than that of DiD-PCNP group (Fig. 2E-F), confirming the good immune escape ability of PCNPs.

3.4 In Vitro Loading and Releasing of β-mangostin by PCNPs

Bare core PCNPs and β-PCNPs were synthesized as outlined in Fig. S1. The encapsulation efficiency (EE) and loading content (LC) of the β-mangostin-loaded PCNPs are summarized in Fig. 3A-B. Although the highest LC (15.1%) was achieved when the mass ratio of β-mangostin : PLGA-NPs was 1:3, the EE was only 75.6%, leading to wastage of β-mangostin. The ratio of 1:4 offers a good balance between these two extremes, with LC and EE of 13.08% and 82.3%, respectively. As shown in Fig. 3C, the stability of the β-mangostin-loaded NPs was evaluated and it was found to exist stably in H_20, PBS, and 10% FBS, with a

particle size of approximately 190 ± 5 nm and PDI < 0.1. The in vitro release profiles of β-mangostin loaded into NPs and PCNPs were investigated using 10% FBS (Fig. 3D).The β-NPs showed a burst of drug release in the initial 8 h of the experiment, and reached a cumulative release of 50.4 ± 6.7% after 24 h. This can be attributed to their porous structures. This burst release was inhibited after coating with the cell membrane, which can be ascribed to the blocking of the β-mangostin release by the compact lipid bilayer at the exterior of the particles.

3.5 In Vitro Anticancer Performance

Next, the in vitro therapeutic effects of β-PCNPs were evaluated. First, the CCK8 assay results demonstrated the biocompatibility of PCNPs (Fig. 3E) and the therapeutic efficacy and targeting ability of β-PCNPs on C6 glioma cells (Fig. 3F). At a β-mangostin concentration of 10 μg/mL, the C6 glioma cells treated with β-PCNP showed significantly low viability as 17.0%, whereas the C6 glioma cell viability of the β-NPs group was up to 47.54%. Furthermore, to study the apoptosis of C6 cells treated with β-PCNPs, the C6 cells were incubated with DMEM, β-NPs, β-PNPs, β-CNPs, and β-PCNPs for 24 h, stained with Annexin V-FITC/PI, and analyzed by flow cytometry. In fact, PI and FITC are known to interfere with each other in the apoptosis assay; therefore, unstained C6 cells and C6 cells stained with Annexin V or PI only were also processed for compensation. Compared with the control groups, β-PCNPs strongly induced the apoptosis of C6 cells. After 24 h of incubation with β-PCNPs, approximately half of the C6 cells were in the late apoptotic stage (Fig. 3G, upper right quadrant, Annexin V, PI+), whereas in the other groups, the percentage of late apoptotic C6 cells was significantly lower. Overall, β-PCNPs possess excellent in vitro antitumor effect on C6 cells, which makes them a promising candidate for in vivo chemotherapy.

3.6 In Vivo Antitumor Activity in Subcutaneous C6 Glioma Model

Based on the encouraging results of the in vitro antitumor activity of β-PCNPs, a subcutaneous C6 glioma model was used to investigate the therapeutic performance of β-PCNPs in vivo. PBS, free β-mangostin, β-NPs, β-PNPs, β-CNPs, and β-PCNPs were injected into tumor-bearing mice through the caudal vein. In all formulations, the same β-mangostin dosage of 25 mg/kg was used. As shown in Fig. 4A, free β-mangostin exhibited little inhibition of tumor growth due to drug resistance, whereas β-NPs, β-PNPs, β-CNPs, and β-PCNPs suppressed the tumor growth to different degrees. During the treatment of the mice, the body weights of the mice in each treatment group were consistent with the change trend of the PBS group (Fig. 4B). No obvious toxic reactions and mouse deaths were observed during the experiment, assuring high biological safety. After sacrifice at the end of the experiment, the tumor tissue was examined after cardiac perfusion with 4% paraformaldehyde (Fig. 4C-D); the size of the tumor was in the order PBS > free β-mangostin > β-NPs > β-PNPs > β-CNPs > β-PCNPs. It is considered that the PLT–C6 hybrid membrane coating on the surface of the PLGA NPs could enhance the uptake by cancer cells and the accumulation of the formulation in the tumor. Immunofluorescent TUNEL staining assay was performed to assess tumor cell apoptosis.The results are presented in Fig. 4E. Green (apoptotic) cells were seen in the animals that received β-PNPs, β-CNPs, or β-PCNPs, but the apoptosis was much more

evident in the β-PCNP treatment group. These results indicate that β-PCNPs can act as an effective drug delivery platform for tumor suppression.

3.7 In Vivo Antitumor Activity in Orthotopic Glioma Model

The construction process of the orthotropic glioma-bearing mouse model is shown in Fig. 5A. In order to analyze the performance of NPs across the blood-brain barrier based on this model, the in vivo distribution of NPs in mice and their accumulation in the brain were measured 24 h after administration (Fig. 5B-C). The NPs could hardly be detected in the brain due to the existence of the BBTB, whereas cell membrane modification increased the accumulation to a greater extent in glioma because the PCNPs could traverse the BBTB by receptor-mediated transcytosis.

Similarly, orthotropic C6 glioma-bearing mice model and survival evaluation were presented in a Kaplan–Meier plot to investigate the in vivo anti-glioma efficacy of β-PCNPs. Mice were randomly divided into six groups and treated with PBS, free β-mangostin, β-NPs, β-PNPs, β-CNPs, and β-PCNPs at a single dose of 5 mg/kg β-mangostin 10 days after implantation of the C6 cell suspension, at which stage the BBTB emerged as the main obstacle for the nanocarriers. As depicted in Fig. 5D, free β-mangostin exhibited only a mild therapeutic effect. Similarly, because of the short half-life and poor specific targeting ability, a limited improvement in efficacy was observed in the β-NP, β-PNP, and β-CNP groups. It is noteworthy that relative to the 26-day median survival time of the untreated group, β-PCNPs significantly prolonged mice survival with a median survival time of 33 days (β-PCNPs vs. all other groups, $p < 0.05$). Brain glioma sections from each group were stained with hematoxylin and eosin (H&E) to observe the tumor growth (Fig. 5E). Furthermore, to evaluate the in vivo biocompatibility and safe of the β-PCNPs, heart, liver, spleen, lung, and kidneys were collected after sacrifice and imaged after H&E staining (Fig. S2). No differences were observed between the control group receiving PBS and the animals treating with β-PCNPs, suggesting the safety of β-PCNPs for in vivo medical applications.

Discussion

Glioma, a common intracranial malignant tumor of the human central nervous system, is highly invasive and has poor prognosis[30]. BBB and BBTB are the biggest obstacles that hamper the delivery of several drugs, thus limiting their efficacy against glioma[31 32]. The discovery of novel and efficient drug delivery systems to break through the BBB and target the glioma cells is highly desired for the treatment of malignant glioma.

In recent years, a number of different strategies have been developed and implemented to overcome the BBB and deliver relevant drugs to brain tumors [33 34]. Lu et al. developed a disulfide bond-conjugated prodrug polymer (CPT-S-S-PEG-iRGD@IR780 micelles) consisting of camptothecin (CPT), polyethylene glycol (PEG), and iRGD peptide, which could effectively cross various barriers to reach the glioma site; moreover, the antitumor effect was significantly enhanced with laser irradiation[35]. Because the capacity of tumor targeting is highly dependent on the corresponding receptor expression density on the surface of the tumor cells[36], we developed hybrid cell membrane-coated NPs, consisting of FDA-certified

degradable PLGA nanospheres, platelet–C6 hybrid membranes, and β-mangostin extracted and purified from mangosteen, which have good bioactivity and biocompatibility for targeting glioma cells for efficient treatment of glioma in situ.

The platelet–C6 cell hybrid membrane-camouflaged NPs (PCNPs) prepared in this study had an average diameter of 130 nm, with a uniform approximately 10-nm-thick outer shell that was indicative of a hybrid membrane. SDS-PAGE results showed that the surface proteins of the cell membranes were completely retained on the nanocarriers, which agrees with the results of previous studies[37]. Several studies have shown that the main anti-tumor responses are associated with the adaptive immune system, which affects the delivery of drugs by immunocytes[38 39]. Flow cytometry and confocal microscopy evaluated the endocytosis of NPs, which have a significant role in the immune escape characteristics of the subsets of the immune system in vitro. We found that PCNPs were taken up by the THP-1 cells to a much lesser extent than NPs, PNPs, and CNPs, but were easily taken up by the C6 cells. Furthermore, in vivo PCNPs extended the blood circulation and further enhanced the tumor targeting of the nanocarriers (Fig. S3). Fluorescence imaging also showed that high accumulation in the brain glioma was obtained at 24 h post tail injection, which was 2.6 times higher than that in cells treated with NPs. The efficiency was similar to that in a recent report, which stated that cancer cell membrane-coated NPs enhance cancer accumulation in camouflaged nanocarriers[40 41].

Apoptosis is programmed cell death, which plays a critical role in maintaining normal development and cell homeostasis[42]. The induction of apoptosis in tumor cells is a promising approach for tumor therapy[43]. Our previous studies have confirmed that the apoptosis of glioma cells by β-mangostin treatment is accompanied by BAX mitochondrial distribution, oligomerization, and caspase 3 activation[28]. The physical and chemical properties of β-mangostin can be effectively improved after encapsulation into NPs by the PCNPs. The CCK8 experiment showed that β-PCNPs significantly inhibited the proliferation of C6 glioma cells when compared with both bare core NPs and cell membrane-coated NPs. β-PCNPs triggered the highest level of apoptosis in C6 cells, indicating that the delivery of β-mangostin, mediated by hybrid membrane-coated NPs, increased the efficacy of cell apoptosis by β-mangostin, which is consistent with the results of the TUNEL assay.

In vivo, the average tumor volume of the β-PCNP group (232.3 ± 49.7 mm^3) on the 18th day of dosing in the C6 subcutaneous tumor model was significantly smaller than that of the untreated group (945.3 ± 199.0 mm^3). To further evaluate the anti-tumor effect of β-PCNPs on the glioma in a clinically relevant model, we transplanted the C6 cells into the right striatum to establish an orthotopic glioma mouse model. The untreated mice had a median survival of 26 days, which is in agreement with the study by Zing et al.[44]. The median survival was 27 days in the anti-PD-1 antibody arm and 28 days in the radiation arm; however, treatment with β-PCNPs prolonged the survival to 33 days in our study. Thus, we have successfully developed hybrid biomimetic camouflaged NPs with multiple targeting capabilities and demonstrated their efficient delivery of β-mangostin to the tumor site. In addition, the developed NPs potently inhibited tumor growth without causing systemic adverse effects.

Conclusion

We generated platelet–cancer cell hybrid membrane-coated hollow PLGA NPs loaded with β-mangostin. These β-PCNPs enhanced chemotherapy against glioma cells through homotypic cell targeting and immune escape. Long-term inhibition of tumor growth and metastasis was achieved owing to the characteristics of the hybrid membrane, and sustained clearance of the tumor cells by β-mangostin was observed. The high biocompatibility and excellent efficacy of β-PCNPs make them highly promising for glioma treatment.

Declarations

ETHICS APPROVAL AND CONSENT TO PARTICIPATE

All animals were raised in SPF level environment. This study has been ethically approved by the Medical Ethics Committee of Zhejiang Provincial People's Hospital. We promise that the project was performed according to the international, national and institutional rules considering animal experiments, clinical studies and biodiversity rights.

CONSENT FOR PUBLICATION

Not applicable.

AVAILABILITY OF DATA AND MATERIALS

All data generated or analysed during this study are included in this published article and its supplementary information files.

COMPETING INTERESTS

The authors declare that they have no competing interests.

FUNDING

This work was supported by grants from the National Natural Science Foundation of China (81772664), Zhejiang Medical and Health Science and Technology Project (2018KY868, 2019KY017). Key projects jointly constructed by the Ministry and the province of Zhejiang Medical and Health Science and Technology Project (WKJ-ZJ-2019). Key and Major Projects of Traditional Chinese Medicine Scientific Research Foundation of Zhejiang Province (2019ZZ001, 2018ZY001). Key projects jointly constructed by the Medicine and Health Research Foundation of Zhejiang Province (WKJ-ZJ-2101).

AUTHORS' CONTRIBUTIONS

LLW: Investigation, Methodology and Writing-original draft. QL: Methodology, Writing-review and editing. JJD, BYC: Investigation, Conceptualization. WDX, YQD: Methodology. WZ, FHG: Data curation, Writing-

review and editing. SYL, JLS: Validation, Investigation. KQL,ZW: Supervision, Project administration, Funding acquisition. All authors read and approved the final manuscript.

ACKNOWLEDGEMENTS

Not applicable.

References

1. Wirsching HG, Galanis E, Weller M. Glioblastoma Handb Clin Neurol. 2016;134:381–97.
2. Ellison DW. Multiple Molecular Data Sets and the Classification of Adult Diffuse Gliomas. N Engl J Med. 2015;372(26):2555–7.
3. Afshari A, Mollazadeh H, Henney N, Jamialahmad T, Sahebkar AJSicb. Effects of statins on brain tumors: a review. Semin Cancer Biol 2020.
4. Fu S, Liang M, Wang Y, et al. Dual-Modified Novel Biomimetic Nanocarriers Improve Targeting and Therapeutic Efficacy in Glioma. ACS Appl Mater Interfaces. 2019;11(2):1841–54.
5. Yang M, Li J, Gu P, Fan XJBm. The application of nanoparticles in cancer immunotherapy: Targeting tumor microenvironment. Bioact Mater. 2021;6(7):1973–87.
6. Shaw T, Mandal D, Dey G, et al. Successful delivery of docetaxel to rat brain using experimentally developed nanoliposome: a treatment strategy for brain tumor. Drug Deliv. 2017;24(1):346–57.
7. Gangapurwala G, Vollrath A, De San Luis A, Schubert UJP. PLA/PLGA-Based Drug Delivery Systems Produced with Supercritical CO-A Green Future for Particle Formulation? Pharmaceutics 2020,12(11):1118.
8. Kang Y, Holley C, Abidian M. Tumor Targeted Delivery of an Anti-Cancer Therapeutic: An In Vitro and In Vivo Evaluation. Adv Healthc Mater. 2021;10(2):e2001261.
9. Huo T, Yang Y, Qian M, et al. Versatile hollow COF nanospheres via manipulating transferrin corona for precise glioma-targeted drug delivery. 2020,260:120305.
10. Cano A, Ettcheto M, Chang J, et al. Dual-drug loaded nanoparticles of Epigallocatechin-3-gallate (EGCG)/Ascorbic acid enhance therapeutic efficacy of EGCG in a APPswe/PS1dE9 Alzheimer's disease mice model. 2019,301:62–75.
11. Luk BT, Zhang L. Cell membrane-camouflaged nanoparticles for drug delivery. J Control Release. 2015;220(Pt B):600–7.
12. Xia Q, Zhang Y, Li Z, Hou X, Feng NJApSB. Red blood cell membrane-camouflaged nanoparticles: a novel drug delivery system for antitumor application. Acta Pharm Sin B. 2019;9(4):675–89.
13. Kang T, Zhu Q, Wei D, et al. Nanoparticles Coated with Neutrophil Membranes Can Effectively Treat Cancer Metastasis. ACS Nano. 2017;11(2):1397–411.
14. Li M, Li J, Chen J, et al. in SituPlatelet Membrane Biomimetic Magnetic Nanocarriers for Targeted Delivery and Generation of Nitric Oxide in Early Ischemic Stroke. 2020,14(2):2024–35.

15. Oroojalian F, Beygi M, Baradaran B, Mokhtarzadeh A, Shahbazi MJS. Immune Cell Membrane-Coated Biomimetic Nanoparticles for Targeted Cancer Therapy. Small 2021:e2006484.
16. Yang R, Xu J, Xu L, et al. Cancer Cell Membrane-Coated Adjuvant Nanoparticles with Mannose Modification for Effective Anticancer Vaccination. ACS Nano. 2018;12(6):5121–29.
17. Wu M, Le W, Mei T, et al. Cell membrane camouflaged nanoparticles: a new biomimetic platform for cancer photothermal therapy. Int J Nanomedicine. 2019;14:4431–48.
18. Wang Y, Luan Z, Zhao C, Bai C, Yang KJEjopsojotEFfPS. Target delivery selective CSF-1R inhibitor to tumor-associated macrophages via erythrocyte-cancer cell hybrid membrane camouflaged pH-responsive copolymer micelle for cancer immunotherapy. Eur J Pharm Sci. 2020;142:105136.
19. Dehaini D, Wei X, Fang R, et al. Erythrocyte-Platelet Hybrid Membrane Coating for Enhanced Nanoparticle Functionalization. Adv Mater 2017,29(16).
20. Ji B, Cai H, Yang Y, et al. Hybrid membrane camouflaged copper sulfide nanoparticles for photothermal-chemotherapy of hepatocellular carcinoma. Acta Biomater. 2020;111:363–72.
21. Cai C, Wu Q, Hong H, et al. In silico identification of natural products from Traditional Chinese Medicine for cancer immunotherapy. Sci Rep. 2021;11(1):3332.
22. Xiong Y, Gao M, van Duijn B, Choi H, van Horssen F, Wang MJPr. International policies and challenges on the legalization of traditional medicine/herbal medicines in the fight against COVID-19. Pharmacol Res 2021:105472.
23. Liao X, Gao Y, Zhao H, et al. Cordycepin Reverses Cisplatin Resistance in Non-small Cell Lung Cancer by Activating AMPK and Inhibiting AKT Signaling Pathway. Front Cell Dev Biol. 2020;8:609285.
24. WM A, FH A-H, research SJSJJoa. Valorization of mangosteen, "The Queen of Fruits," and new advances in postharvest and in food and engineering applications: A review. J Adv Res. 2019;20:61–70.
25. Huang CF, Teng YH, Lu FJ, et al. β-mangostin suppresses human hepatocellular carcinoma cell invasion through inhibition of MMP-2 and MMP-9 expression and activating the ERK and JNK pathways. Environ Toxicol. 2017;32(11):2360–70.
26. Lee K, Ryu H, Oh S, et al. Depigmentation of α-melanocyte-stimulating hormone-treated melanoma cells by β-mangostin is mediated by selective autophagy. Exp Dermatol. 2017;26(7):585–91.
27. CS L, CL L, TH Y, et al. β-Mangostin inhibits the metastatic power of cervical cancer cells attributing to suppression of JNK2/AP-1/Snail cascade. J Cell Physiol 2020.
28. Li K, Wu L, Chen Y, et al. Cytotoxic and Antiproliferative Effects of β-Mangostin on Rat C6 Glioma Cells Depend on Oxidative Stress Induction via PI3K/AKT/mTOR Pathway Inhibition. Drug Des Devel Ther. 2020;14:5315–24.
29. Zhou H, Fan Z, Lemons P, Cheng HJT. A Facile Approach to Functionalize Cell Membrane-Coated Nanoparticles. Theranostics. 2016;6(7):1012–22.
30. Li J, Liu X, Qiao Y, et al. Association Between Genetic Variant in the Promoter of Pri-miR-34b/c and Risk of Glioma. Front Oncol. 2018;8:413.

31. Jiao X, Yu Y, Meng J, et al. Dual-targeting and microenvironment-responsive micelles as a gene delivery system to improve the sensitivity of glioma to radiotherapy. Acta Pharm Sin B. 2019;9(2):381–96.
32. Zeiadeh I, Najjar A, Karaman R. Strategies for Enhancing the Permeation of CNS-Active Drugs through the Blood-Brain Barrier: A Review. Molecules 2018,23(6).
33. Zhou X, Smith Q. Liu XJWirN, nanobiotechnology. Brain penetrating peptides and peptide-drug conjugates to overcome the blood-brain barrier and target CNS diseases. Wiley Interdiscip Rev Nanomed Nanobiotechnol 2021:e1695.
34. Su Z, Xing L, Chen Y, et al. Lactoferrin-modified poly(ethylene glycol)-grafted BSA nanoparticles as a dual-targeting carrier for treating brain gliomas. Mol Pharm. 2014;11(6):1823–34.
35. Lu L, Zhao X, Fu T, et al. An iRGD-conjugated prodrug micelle with blood-brain-barrier penetrability for anti-glioma therapy. Biomaterials. 2020;230:119666.
36. Ferraris C, Cavalli R, Panciani P, Battaglia LJIjon. Overcoming the Blood-Brain Barrier: Successes and Challenges in Developing Nanoparticleï»¿-Mediated Drug Delivery Systems for the Treatment of Brain Tumours. 2020,15:2999–3022.
37. He H, Guo C, Wang J, et al. Leutusome: A Biomimetic Nanoplatform Integrating Plasma Membrane Components of Leukocytes and Tumor Cells for Remarkably Enhanced Solid Tumor Homing. Nano Lett. 2018;18(10):6164–74.
38. Jia Y, Wang X, Hu D, et al. Phototheranostics: Active Targeting of Orthotopic Glioma Using Biomimetic Proteolipid Nanoparticles. ACS Nano. 2019;13(1):386–98.
39. Chen Z, Zhao P, Luo Z, et al. Cancer Cell Membrane-Biomimetic Nanoparticles for Homologous-Targeting Dual-Modal Imaging and Photothermal Therapy. ACS Nano. 2016;10(11):10049–57.
40. Han L, Xu Y, Guo X, Yuan C, Mu D, Xiao Y. Cancer cell membrane-coated biomimetic platform for targeted therapy of breast cancer in an orthotopic mouse model. J Biomater Sci Polym Ed. 2020;31(12):1538–51.
41. Wang H, Wu J, Williams GR, et al. Platelet-membrane-biomimetic nanoparticles for targeted antitumor drug delivery. J Nanobiotechnology. 2019;17(1):60.
42. Xu X, Lai Y, Hua ZC. Apoptosis and apoptotic body: disease message and therapeutic target potentials. Biosci Rep 2019,39(1).
43. Lu W, Sun Q, Chen B, Li Y, Xu Y, Wang S. Novel agent #2714 potently inhibits lung cancer growth by suppressing cell proliferation and by inducing apoptosis in vitro and in vivo. Mol Med Rep. 2019;19(6):4788–96.
44. Zeng J, See AP, Phallen J, et al. Anti-PD-1 blockade and stereotactic radiation produce long-term survival in mice with intracranial gliomas. Int J Radiat Oncol Biol Phys. 2013;86(2):343–9.

Figures

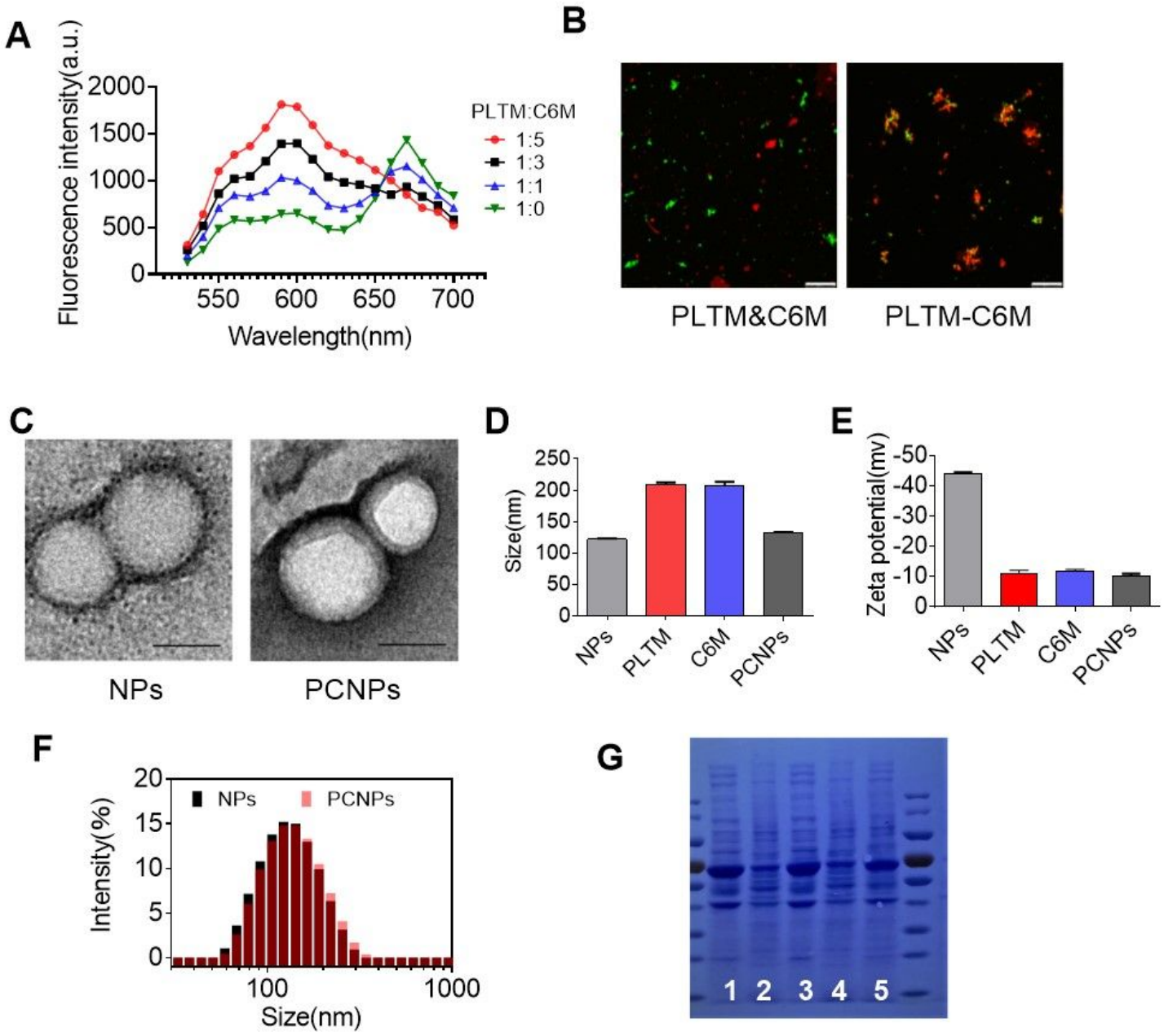

Figure 1

Fabrication and physicochemical characterization of PCNPs. (A) Platelet membrane was doped with a pair of FRET membrane probes and fused with increasing amounts of C6 cell membrane. The recovery of fluorescence emission from the donor was monitored at the lower emission peak (525 nm, PLTM : C6M = platelet membrane protein to C6 cell membrane ratio). (B) laser scanning confocal microscopy images of either a mixture of PNPs and CNPs or of the PCNPs (red = C6 cell membrane, green = platelet membrane; scale bar = 10 μm). (C) Representative TEM images of bare PLGA cores and PCNPs, negatively stained with vanadium (scale bar = 100 nm). (D-E) Z-average size and surface zeta potential of bare PLGA cores, PNPs, CNPs, and PCNPs, as measured by DLS. (F) Z-average size of bare PLGA cores and PCNPs. (G) Protein content visualization of 1: platelet, 2: C6 cells, 3: PNPs, 4: CNPs, and 5: PCNPs, run on SDS

polyacrylamide gel electrophoresis at equivalent protein concentrations followed by Coomassie brilliant blue staining. Data are represented as mean ± S.D of three independent experiments.

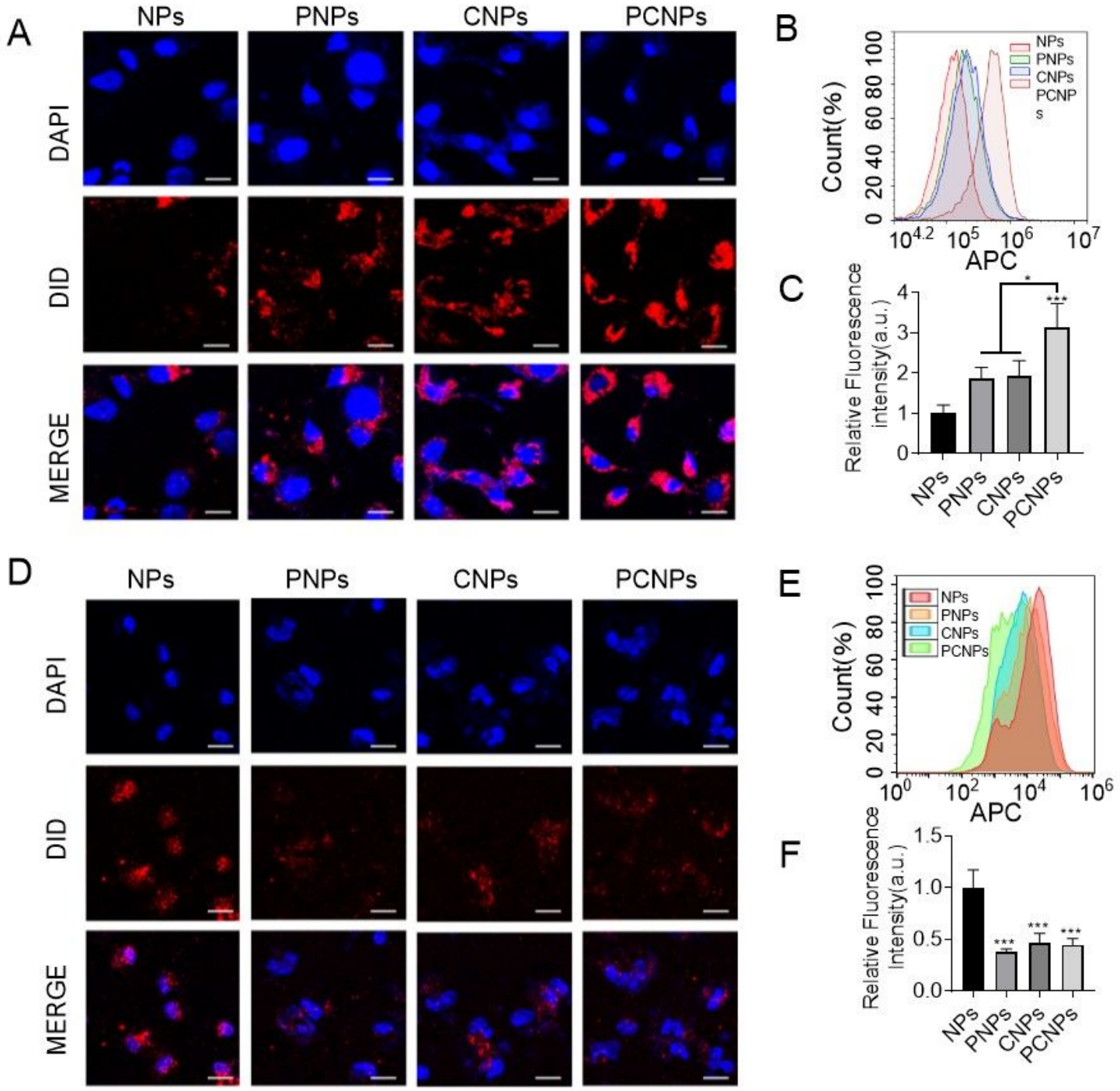

Figure 2

Homotypic targeting and immune escape ability of β-PCNPs. (A) Confocal fluorescence imaging of dye-labeled bare PLGA cores, P-NPs, C-NPs, and P-C-NPs after incubation with C6 cells (red = nanoparticles, blue = nuclei; scale bars = 20 μm). (B-C) Binding of fluorescently labeled bare PLGA cores, P-NPs, C-NPs, and P-C-NPs to C6 glioma cells, as analyzed by flow cytometry. (D) Confocal fluorescence imaging of

dye-labeled bare PLGA cores, P-NPs, C-NPs, and P-C-NPs after incubation with THP-1 cells (red = nanoparticles, blue = nuclei; scale bars = 20 μm). (E-F) The uptake of fluorescently labeled bare NPs, P-NPs, C-NPs, and P-C-NPs when incubated with human macrophage-like cells, as analyzed by flow cytometry. Data are represented as mean ± S.D of three independent experiments; *P < 0.05, ***P<0.001.

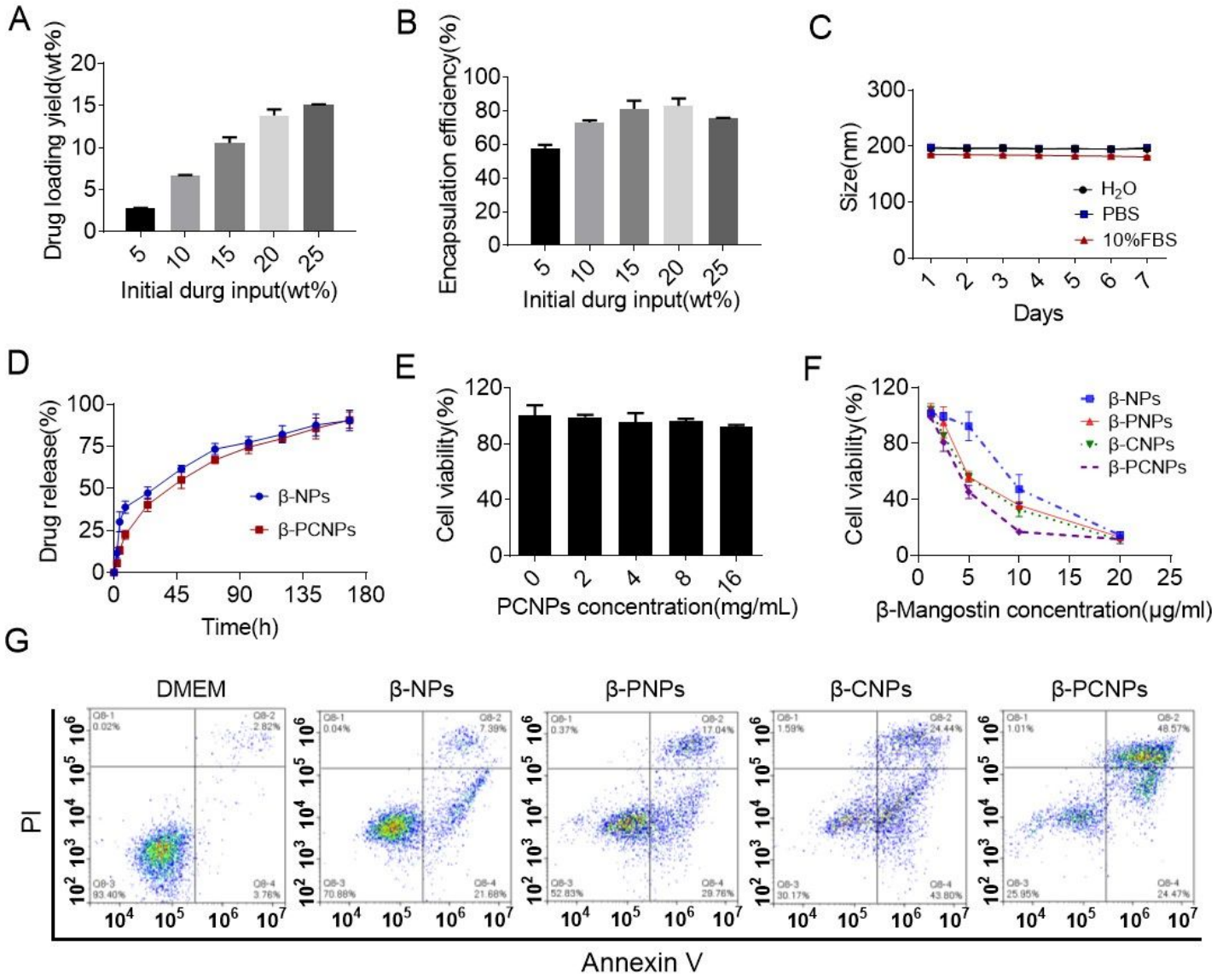

Figure 3

In vitro anti-tumor activity of different nanoparticles. (A-B) β-Mangostin loading capacity and encapsulation efficiency of PCNPs when the β-mangostin concentration was 75, 150, 225, 300, and 375 μg/mL. (C) Z-average size of PCNPs over 7 days in water, PBS, and 10％FBS. (D) β-Mangostin release from β-NPs and β-PCNPs at 10％FBS. (E) CCK8 assay is used to measure cell viability in HT22 with different concentrations of PCNPs. (F) CCK8 assay is used to measure cell viability rate in C6 cells with different concentrations of β-PCNPs. (G) C6 cell apoptosis is measured using flow cytometry. Data are represented as mean ± S.D of three independent experiments.

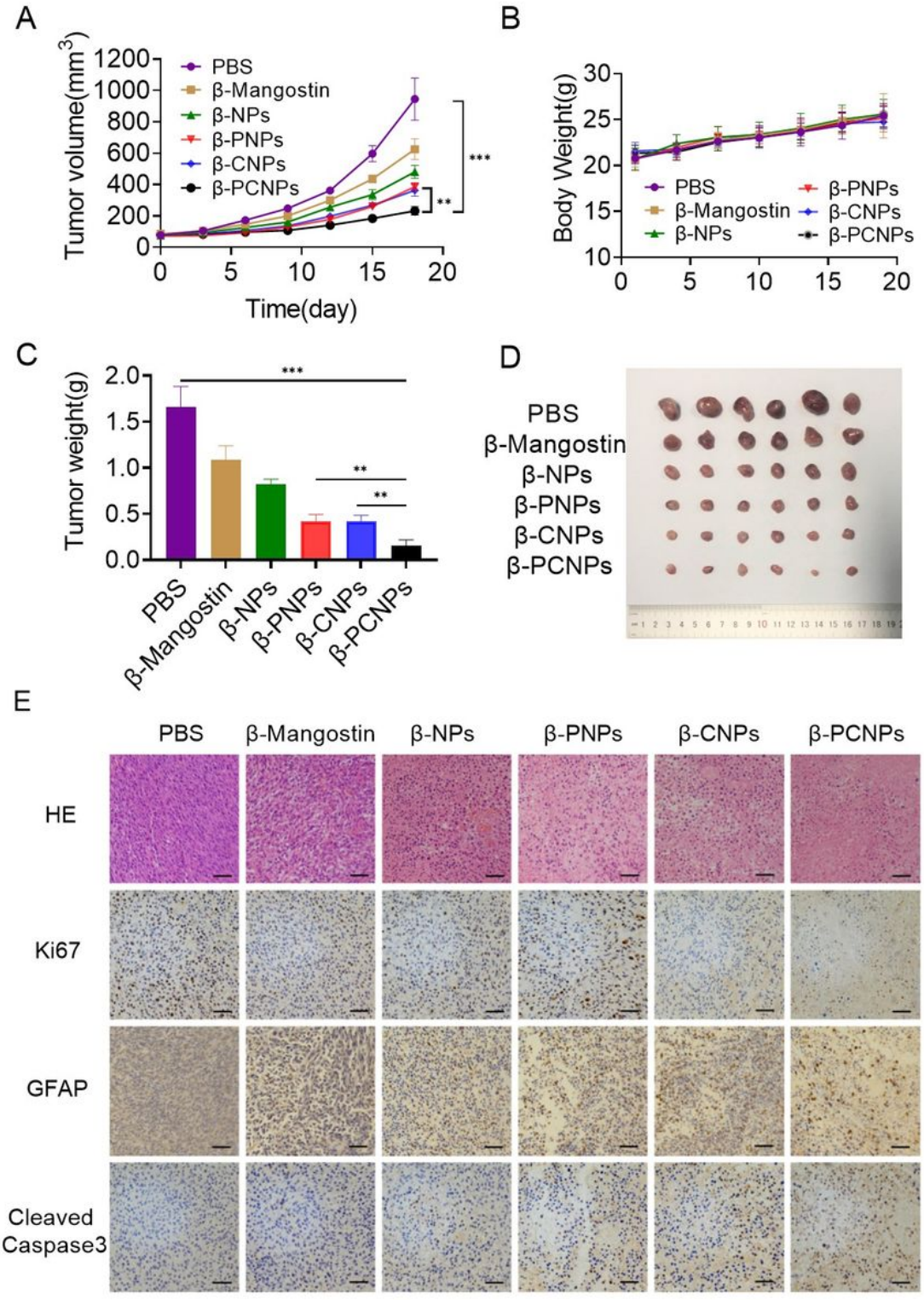

Figure 4

β-Mangostin-loaded nanoparticles inhibit the growth of glioma cells in a subcutaneous transplantation tumor model of C6 cells. (A) Relative tumor volume, (B) body weight, and (C) tumor weight of bearing mice receiving different treatments. (D) Images of tumors in each tested group. (E) H&E staining, immunohistochemical detection, and TUNEL assay of tumor tissues in different groups (scale bar = 200 μm). Data are presented as the mean ± S. D. of three independent experiments; **P < 0.01, ***P<0.001.

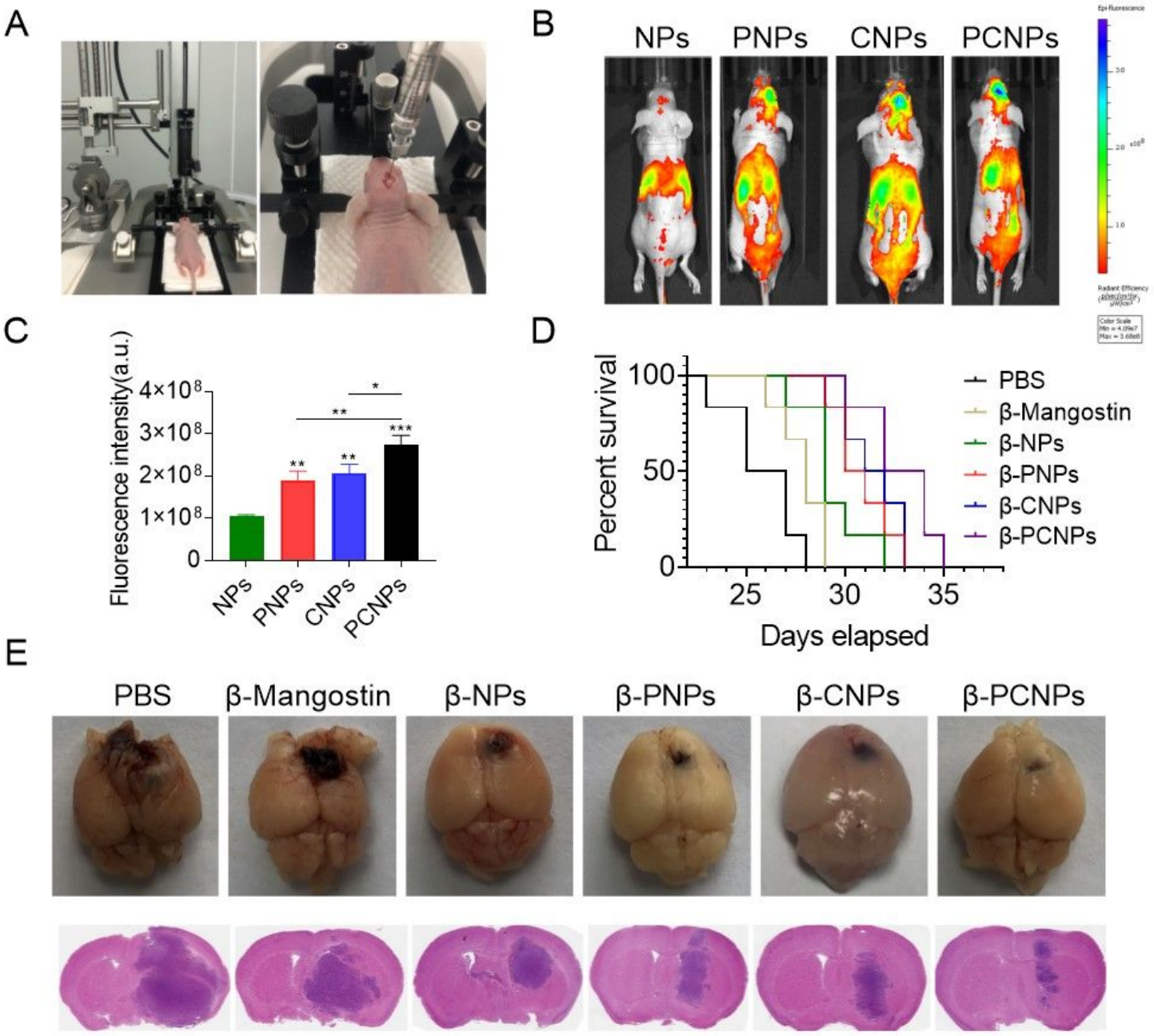

Figure 5

β-Mangostin-loaded nanoparticles inhibit the growth of glioma cells in an orthotopic glioma model. (A) Schematic diagram of glioma model. (B) Representative fluorescence images of orthotopic C6 glioma mouse models from different groups. (C) Quantitative fluorescence signal intensity in the brain. (D) Survival rate curves for each test group. (E) Schematic diagram of tumors and H&E staining of brain sections from all groups on day 20. Data are presented as the mean ± S. D. of three independent experiments; *P < 0.05, **P < 0.01, ***P <0.001.

Supplementary Files

This is a list of supplementary files associated with this preprint. Click to download.

- renamed5f3d5.pdf
- Supplementarydata.docx